Available online at www.sciencedirect.com
SCIENCE DIRECT®
Fire Safety Journal 39 (2004) 217–238
FIRE SAFETY JOURNAL
www.elsevier.com/locate/firesaf

The effect of water sprays on fire fighter thermal imagers

John F. Widmann*, Jason Duchez[1]

Building and Fire Research Laboratory, National Institute of Standards and Technology, Gaithersburg, MD 20899-8663, USA

Received 8 April 2003; received in revised form 2 September 2003; accepted 17 November 2003

Abstract

The performance of fire fighter thermal imagers through water sprays has been investigated experimentally and theoretically. Thermal imagers are finding increasing use in fire fighting applications, and the ubiquitous nature of fire sprinklers, water mist suppression systems, and water curtains for radiation attenuation necessitates a thorough understanding of the effect of water sprays and mists on thermal imager performance. Laboratory-scale and full-scale evaluations of thermal imager performance through water sprays have been conducted, and the results analyzed using Mie theory to predict the extinction of radiation by water drops. Imagers were found to perform satisfactorily even through water sprays produced by sprinkler nozzles with *K*-factors as large as $6.0 \times 10^{-4}\,\mathrm{m^3\,s^{-1}\,kPa^{-0.5}}$ ($25\,\mathrm{gal\,min^{-1}\,psi^{-0.5}}$). Tests were conducted under non-fire conditions; thus, the effect of interaction between water sprays and a hot smoke layer on imager performance was not investigated.
Published by Elsevier Ltd.

Keywords: Thermal imagers; Infrared imagers; Water sprays; Radiation extinction

1. Introduction

Thermal imagers represent an important application of emerging technology for increasing safety and efficiency in fire fighting. Taking advantage of greater optical depth in the infrared region of the electromagnetic spectrum compared to the visible

*Corresponding author. Current address: Fluent Inc., Lebanon, NH, USA. Tel.: +1-603-643-2600; fax: +1-603-643-3967.
E-mail address: jfw@fluent.com (J.F. Widmann).
[1] Guest researcher. Also affiliated with the Department of Physics, University of Maryland, College Park.

0379-7112/$ - see front matter Published by Elsevier Ltd.
doi:10.1016/j.firesaf.2003.11.006

Nomenclature

c	speed of light in vacuo ($2.9979 \times 10^8\,\mathrm{m\,s^{-1}}$)
D_i	drop diameter of the ith size class
h	Planck's constant ($6.6261 \times 10^{-34}\,\mathrm{J\,s}$)
I	intensity of transmitted radiation
I_0	intensity of incident radiation
k	Boltzmann's constant ($1.3807 \times 10^{-23}\,\mathrm{J\,K^{-1}}$)
K	K-factor or orifice coefficient
L	path length
N_i	number density of drops in the ith size class
N	number of replicated measurements
Q_{ext}	extinction efficiency
s	standard deviation of replicated measurements
T	temperature
x	spatial dimension along the optical path

Greek letters

ε	emissivity
λ	wavelength
τ	transmission, I/I_0

region, thermal imagers enable fire fighters to "see though" smoke-filled rooms. Fire fighters use thermal imagers for search and rescue, locating fires, locating escape routes, and locating hot spots that might re-ignite in both indoor and outdoor applications.

Due to the obvious advantages and increasing use of fire fighter thermal imagers, there is a need for greater understanding of the factors that affect the performance of thermal imagers, and to develop standard procedures for testing and evaluating such devices. Such an effort is underway at the National Institute of Standards and Technology (NIST), where a facility has been built to permit the development of standard test protocols and quantitative metrics to evaluate thermal imager performance under a variety of conditions. This paper reports on one study associated with that effort. In particular, the effect of water sprays on fire fighter thermal imager performance has been investigated.

2. Theory

2.1. Infrared imaging

Thermal imagers are valuable for fire fighting applications because the optical depth in smoke-filled enclosures is much greater for infrared radiation than for

visible radiation. That is, the attenuation of the radiation due to smoke particles is significantly greater for short wavelength (visible) radiation than for long wavelength (infrared) radiation.

In general, infrared imaging systems are classified into four wavelength regions. The near infrared (NIR) spectral range covers the wavelength range from 0.7 to 1.1 μm. The short wavelength infrared (SWIR) band covers the range from 1.1 to 2.5 μm. The wavelength range from 2.5 to 7.0 μm corresponds to the mid-wavelength infrared (MWIR) spectral region. The long wavelength infrared (LWIR) band covers the range from 7 to 15 μm, and is the spectral region in which fire fighter thermal imagers operate. Finally, the fourth infrared region corresponds to the far infrared (FIR), also called the very long wavelength infrared (VLWIR) region, and applies to systems with spectral responses that extend beyond 15 μm [1].

There are two important reasons why fire fighter thermal imagers utilize detectors with spectral responses covering the LWIR band: (i) sufficient emission from objects at ambient temperatures, and (ii) minimal extinction due to ambient gases and particles. Unlike typical imaging applications utilizing visible radiation, fire fighter thermal imagers are designed to measure radiation that is emitted from objects rather than radiation that is scattered by the objects in the scene. Furthermore, they are designed to detect radiation emitted from objects corresponding to a particular temperature range. Infrared imagers designed for fire fighting applications must also provide sufficient contrast so that fire fighters can identify objects (doors, windows, people, fires, etc.) in the image.

Fig. 1 presents the radiant intensity emitted from a black body source calculated from Planck's spectral distribution law for representative temperatures important in enclosure fires. Planck's spectral distribution law is given by [2]

$$I(\lambda, T) = \frac{8\pi hc\varepsilon}{\lambda^5} \frac{1}{\exp(hc/\lambda kT) - 1}, \tag{1}$$

where, λ and T are the wavelength and temperature, respectively. The constants h, k, and c correspond to Planck's constant, Boltzmann's constant, and the speed of light in a vacuum, respectively. A black body corresponds to a surface with unity emissivity, ε. In reality, objects are not perfect emitters and will have surfaces with $\varepsilon < 1$. However, this is generally not a significant issue in fire fighter thermal imaging applications unless the objective is to obtain quantitative temperature information. The effect of $\varepsilon < 1$ on the radiant emission is to scale the curves in Fig. 1 downward, but not to alter the shape of the curves (assuming that the wavelength dependence of ε can be neglected, which corresponds to the gray body approximation).

The curves in Fig. 1A correspond to radiation emission from objects at approximately room temperature (20°C) and body temperature (38°C). It is this difference in emission intensity that enable thermal imagers to obtain images with sufficient contrast to recognize humans in smoke-filled environments. Differences in surface emissivity also contribute to image contrast. The curves in Fig. 1A also show that the spectral distributions of emitted radiation from room-temperature and body-temperature objects peak in the LWIR region of the spectrum. As discussed above, the curves presented correspond to $\varepsilon = 1$. Because the intensity of the emitted

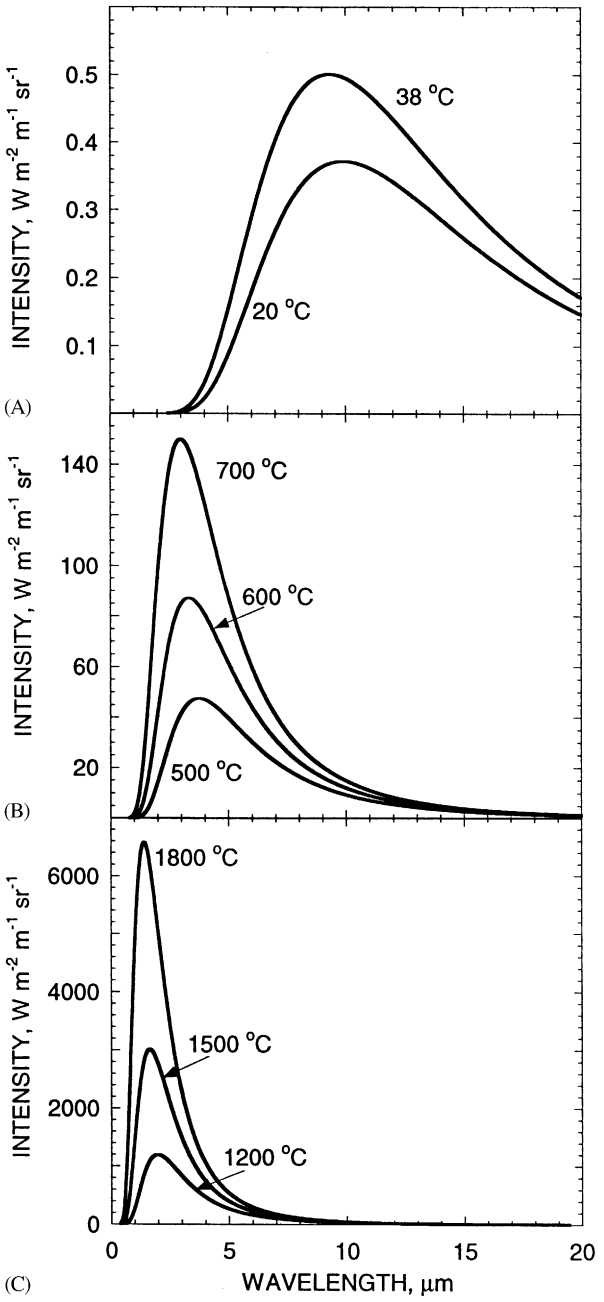

Fig. 1. Radiant intensity with respect to wavelength for black body emitters at temperatures relevant to thermal imager applications in enclosure fires. Typical temperatures corresponding to (A) people and backgrounds, (B) upper smoke layers, and (C) fires are presented.

radiation depends linearly upon the emissivity, hotter objects do not *always* emit more radiation than colder objects. This can be both advantageous and disadvantageous. For example, although unknown emissivity values make quantitative temperature measurements difficult, differences in emissivity permit images to be obtained with sufficient contrast from objects of uniform temperature. Thus, fire fighters may be able to use thermal imagers to locate a door in a smoke-filled enclosure even if the door and surrounding wall correspond to the same temperature.

Figs. 1B and 1C present intensity distributions calculated from Planck's law for temperatures relevant to hot upper layers in enclosure fires and fire sources, respectively. The peaks in the intensity curves shift to shorter wavelengths for increasing temperature. Thus, objects significantly hotter than body-temperature display spectral emission distributions that peak at wavelengths lower than room-temperature and body-temperature objects. Nonetheless, the emission from these objects in the LWIR range is sufficient to overwhelm the emission from colder objects. This is shown more clearly in Fig. 2, where the eight curves presented in Fig. 1 are shown on one plot. Fig. 2 demonstrates why fire fighter thermal imagers can successfully "see through" cooler smoke but are unable to penetrate hot smoke.

The second reason why fire fighter thermal imagers operate in the LWIR region of the electromagnetic spectrum, in addition to the spectral dependence of the thermal emission from room-temperature and body-temperature objects, is the increased optical depth for radiation of this wavelength range through typical gases and particles encountered in fire fighting. The LWIR band corresponds to a region of minimal absorption by atmospheric gases, including CO_2 and H_2O [1]. This makes the LWIR range attractive for operation in enclosures filled with combustion products. Furthermore, the optical extinction due to scattering and absorption by smoke particles decreases with increasing wavelength [3,4]. Thus, from the standpoint of the participating media encountered in fire fighting applications, the LWIR region is very attractive.

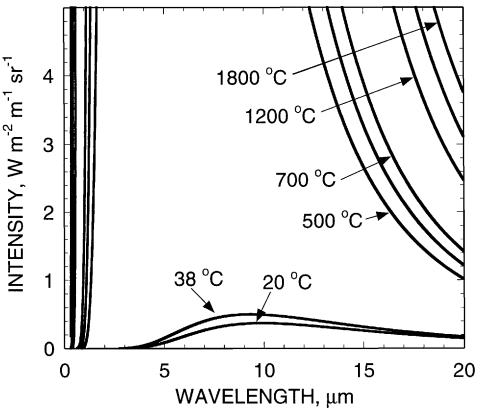

Fig. 2. Radiant intensity for black body emitters at temperatures relevant to thermal imager applications in enclosure fires.

2.2. Radiation attenuation by water sprays

To predict the effect of water sprays on thermal imager performance, it is necessary to determine the fraction of infrared radiation that will be transmitted through the spray. The transmission of infrared radiation through a water spray can be predicted using Mie theory [5] if the spray characteristics are known. Provided that the spray is not too dense, multiple scattering can be neglected and the radiation attenuation can be calculated by summing the contributions of individual drops along the optical path [5,6]. Bayvel and Jones [7] suggest that multiple scattering can be neglected if the path length through the spray is less than the optical mean free path. This corresponds to a minimum transmission of approximately 40%. In general, neglecting multiple scattering is valid for the case of fire sprinkler sprays because such sprays are very dilute (i.e., the number density of drops per unit volume is very low [8,9]). In fact, it has been reported that multiple scattering can be neglected for many spray of practical interest [10], and thus summing the contributions from individual drops along the optical path is a reasonable approach for other drop dispersions encountered in fire fighting applications (e.g., water mists, and rain drops).

In general, the extinction efficiency for spherical drops is a function of wavelength, complex refractive index, and drop size. Furthermore, the drop size distribution and number density will vary with position within a spray. Thus, for a polydisperse spray with spatially varying characteristics, the transmission of radiation in a given direction can be determined from

$$\ln[\tau(\lambda)] = \ln\left(\frac{I(\lambda)}{I_0(\lambda)}\right) = -\int_0^L \left[\sum_i \left(n_i(D_i,x)Q_{\text{ext}}(D_i,\lambda)\frac{\pi D_i^2}{4}\right)\right] \mathrm{d}x, \tag{2}$$

where it is understood that x is a variable of integration corresponding to the spatial dimension along the optical path. Here, n_i is the number density per unit volume for drops in the ith size class; D_i is the drop diameter corresponding to the ith size class; and Q_{ext} is the optical extinction efficiency. The sum on the right-hand side of Eq. (2) corresponds to a summation of all drop size classes and is more convenient than the equivalent integral expression because experimental size distribution data is generally in the form of discrete size classes.

Eq. (2) can be used to predict the transmission of radiation through a spray provided the effects of forward-scattering and in-scattering can be neglected. Forward-scattering refers to radiation that is scattered by drops into the direction of the detector (small scattering angles), and thus results in a decrease in the effective extinction efficiency. Forward-scattering will be negligible for the thermal imagers considered here due to the small size of individual pixels and long distance between the spray and detector [6]. Radiation that is scattered into the direction of the detector from other directions corresponds to in-scattering. In-scattering can significantly reduce the effective extinction efficiency; however, in imaging

applications in-scattering contributes the the noise in the image and not the signal. The effect of in-scattering is discussed further below.

Application of Eq. (2) requires knowledge of the drop size distribution, $\{D_i\}$, and number density, n_i, as a function of position within the spray (along the optical path). Because these parameters depend upon the complicated atomization process, they cannot be predicted reliably from theory and must be determined experimentally. In contrast, the optical extinction efficiency can be calculated as a function of drop size and radiation wavelength using Mie theory, which describes the interaction of a plane wave of electromagnetic radiation with a sphere of uniform refractive index [5]. There is an extensive literature on the use of Mie theory to predict the scattering, absorption, and extinction of radiation by homogeneous spheres, and the reader is referred to the works of van de Hulst [3], Kerker [11], and Bohren and Huffman [12] for comprehensive descriptions of the theory.

The use of Mie theory to predict the optical extinction efficiency of water drops requires knowledge of the complex index of refraction, m, as a function of wavelength. The data of Segelstein [13] were used here. Fig. 3 presents the plots of the real and imaginary parts of the refractive index for water over the wavelength range 0.5–15 μm. The lines correspond to the original data of Segelstein, while the square symbols indicate the values used in this study.

Fig. 4 presents the calculated values of the optical extinction efficiency, Q_{ext}, with respect to wavelength and drop diameter. The calculations correspond to the wavelengths presented in Fig. 3 and drop diameters ranging from 1 to 200 μm. Note that the extinction efficiency reaches an asymptotic value of 2.0 for large values of the drop diameter. Thus, the calculations here, which incorporate the wavelength dependence of m, can be used for predictions of radiation transport in sprays with larger drop sizes (e.g., fire sprinkler sprays [8,9]). A condensed version of the data presented in Fig. 4 has been tabulated in Table 3 of the appendix. The tabulated data include all of the wavelengths used, but only a subset of the drop diameters. The calculations cover the entire wavelength range relevant to thermal imager applications.

3. Experimental

Laboratory- and full-scale measurements have been conducted to evaluate the effect of water sprays on thermal imager performance. Fig. 5 presents a schematic of the experimental facility used for the laboratory-scale tests. The enclosure consists of a metal, bottomless box 1.8 m long, 0.8 m wide, and 1.2 m tall. Windows are located on either end of the enclosure so that an image of a well-defined target can be obtained with the thermal imagers as shown in Fig. 5. ZnSe was chosen for the window material because it transmits radiation over the LWIR region. The windows are 50 and 75 mm in diameter, with the larger window being on the side of the enclosure near the target. The target consists of a series of hot and cold lines created by positioning cold tubes in front of a hot plate. This results in a pattern of alternating hot and cold lines that provide a temperature contrast for imaging similar

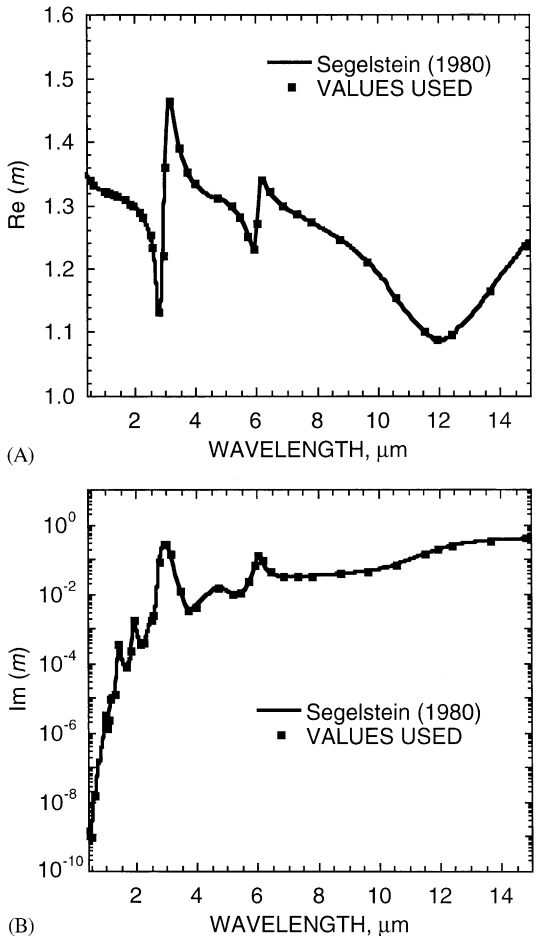

Fig. 3. Values of the complex refractive index for water used in the calculations: (A) real and (B) imaginary components are presented.

to black and white targets used to characterize visible imaging systems [1,14]. The hot plate and copper tubing through which the cold water flows have been painted with flat, black paint to be of consistent emissivity and minimize reflections that could interfere with the measurements. The data presented here corresponds to conditions when the hot plate and cold tubes were maintained at $52^{\circ}C \pm 1^{\circ}C$, and $11^{\circ}C \pm 1^{\circ}C$, respectively. The total distance between the thermal imager and the cold tubing of the target is 2.0 m, with the hot plate being an additional 0.1 m behind the tubing.

Laser extinction measurements were also performed to determine the transmission of visible radiation through the spray for comparison with measurements obtained at infrared wavelengths. For these measurements, a He–Ne laser that emits red light at $\lambda = 0.6328\,\mu m$ was used in place of the thermal imager shown in Fig. 5. The target

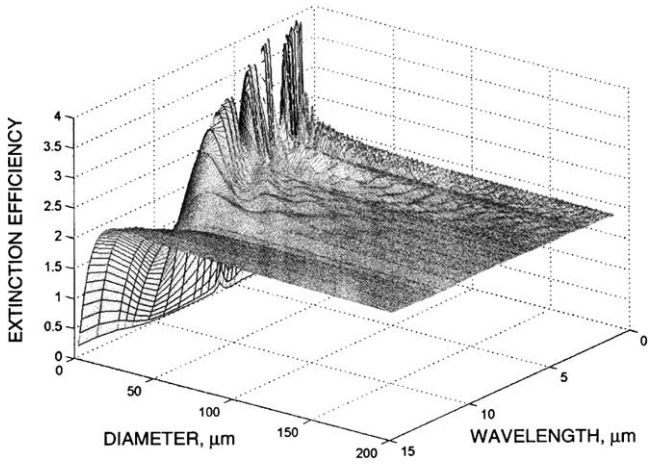

Fig. 4. Calculated values of the extinction efficiency, Q_{ext}, with respect to drop size and radiation wavelength.

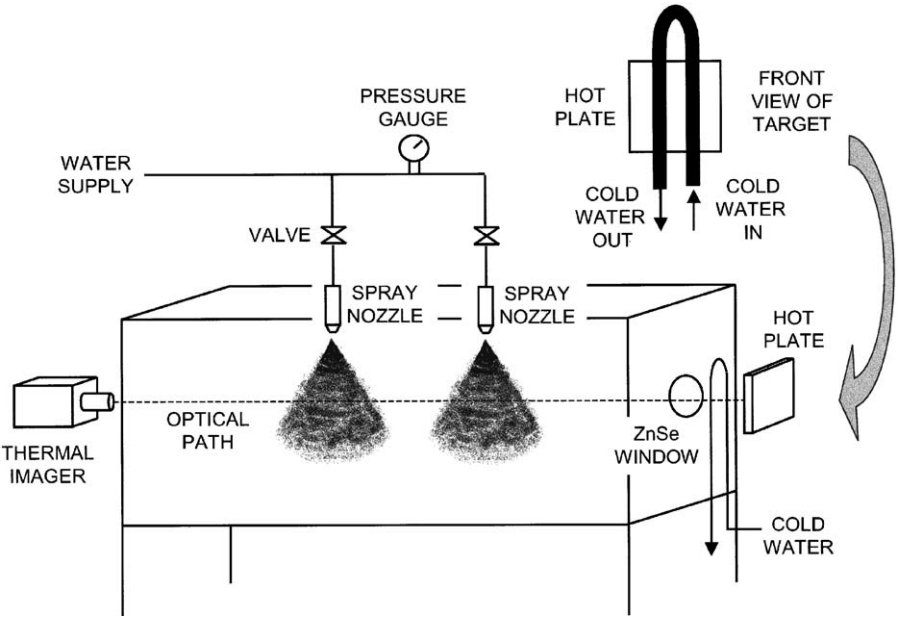

Fig. 5. Schematic of the experimental facility used for the laboratory-scale measurements.

was also replaced by a silicon photodiode detector to measure the intensity of the laser beam.

The laboratory-scale optical extinction measurements presented here correspond to the transmission of radiation through water sprays produced by pressure-swirl

Table 1
Thermal imagers used in this study

Imager	Type	Detector	Array size	Field of view	Spectral response (μm)
A	Scientific	PtSi	256 × 256 pixels	16°	3.4–5.0
B	Fire fighter	Barium strontium titanate (BST)	328 × 245 pixels	59°	8–14
C	Fire fighter	Vanadium oxide microbolometer	320 × 240 pixels	55°	8–14

atomizer nozzles (Delavan,[2] Type B-1.0, 60° cone angle). The spray characteristics were measured using phase Doppler interferometry (PDI), the details of which are available elsewhere [6]. PDI, which is an extension of laser Doppler velocimetry that measures both drop size and velocity, involves creating an interference pattern consisting of alternating light and dark fringes in the region where two laser beams intersect. The region where the beams intersect makes up the probe volume, and drops passing through the probe volume scatter light that exhibits angular intensity distributions characteristic of the size, refractive index, and velocity of the drops. For drops with known refractive index, the size and velocity can be determined by analyzing the scattered light collected with several photomultiplier tubes. Drop volume flux and number density can also be determined using PDI; however, the uncertainties in these measurements are generally larger than the uncertainties in size and velocity measurements. The two nozzles shown in Fig. 5 were located so that the center of the optical path (determined by the windows) was approximately 50 mm beneath the nozzle tip. This was done so that the optical path would correspond to the locations in the spray where the PDI data were obtained [6].

Three thermal imagers were used for the tests presented here. The characteristics of the three imagers are summarized in Table 1. Imager A corresponds to an infrared imager designed for quantitative experimental measurements, whereas the other two imagers were commercially available systems specifically designed and marketed for fire fighting applications. The three imagers utilize different detector technologies, and the scientific imager is sensitive to a different wavelength region than the two fire fighter thermal imagers. Also, the smaller field of view of the scientific infrared camera provides greater spatial resolution than the two fire fighter thermal imagers.

4. Results and discussion

4.1. Laboratory-scale tests

Fig. 6 presents images obtained with the three thermal imagers without a water spray, with a single spray, and with two sprays in the optical path. The white circle

[2] Certain commercial equipment, instruments, or materials are identified in this paper to specify adequately the experimental procedure. Such identification does not imply recommendation or endorsement by the National Institute of Standards and Technology, nor does it imply that the materials or equipment are necessarily the best available for this purpose.

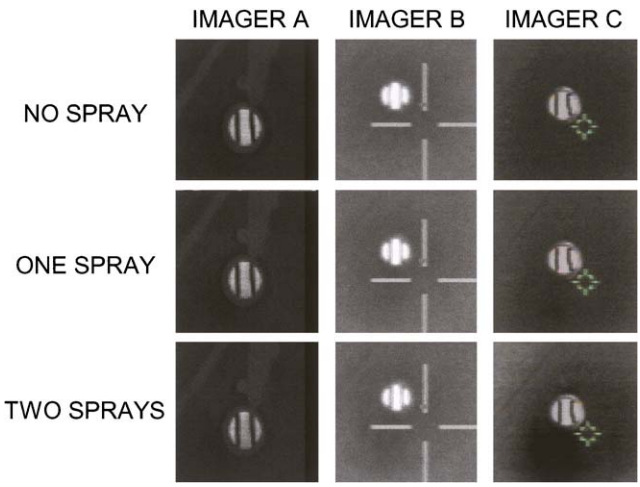

Fig. 6. Images of a well-defined target obtained with three thermal imagers.

with the two vertical lines in the center of each image corresponds to the target as seen though the ZnSe window. The images presented in Fig. 6 demonstrate the effect of automatic detector gain and irises, important features of fire fighter thermal imagers. Imager A does not have an automatic iris or an automatic detector gain, and the decrease in radiation reaching the detector from the target is observed as the sprays are introduced into the optical path. When moving down Fig. 6, the images corresponding to imager A display reduced contrast between the hot and cold "lines" corresponding to the hot plate and the cold tubing, respectively.

The laboratory-scale water sprays used when collecting the images in Fig. 6 have been characterized experimentally using PDI. The measured distributions of drop size and number density were used to predict the transmission of infrared radiation through the spray. Also, the transmission of infrared radiation was measured directly over the wavelength range from 3.0 to 4.0 μm using an infrared spectrograph [6]. The measured and predicted transmissions with respect to wavelength are presented in Fig. 7. The filled square symbol represents the data from Ref. [6] averaged over the wavelength range of the measurements. The data correspond to transmission measurements obtained 50 mm downstream of the nozzle orifice. The predictions correspond to both one and two sprays, and also show the effect of in-scattering. The data in Fig. 7 indicate that in-scattering has a significant effect on the transmission, and should be considered when performing transmission measurements like the ones presented here. However, it should be emphasized that in imaging applications in-scattering leads to additional noise in the image, rather than increased signal. In-scattering results in additional radiation being measured by detector pixels (image plane) that did not originate from the locations in the scene corresponding to those pixels (object plane).

The images corresponding to imager A presented in Fig. 6 can be used to calculate the transmission through the water spray for comparison with the data obtained

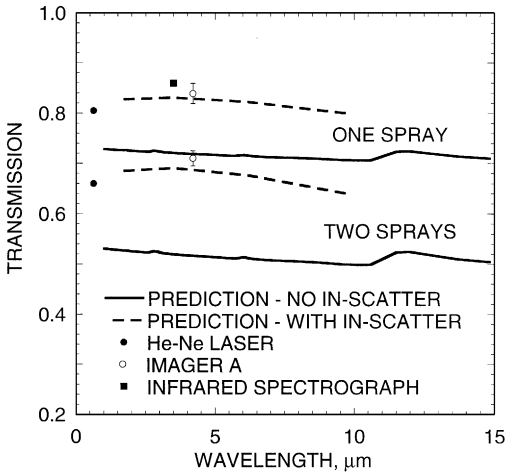

Fig. 7. Comparison of measured and predicted transmissions, I/I_0, with respect to wavelength for the laboratory-scale water spray.

previously using the infrared spectrograph. The open circles in Fig. 7 correspond to the transmission calculated from the images obtained with imager A, and the error bars represent the standard deviation of replicated measurements, s. Note that only the images obtained with imager A can be used to calculate the transmission because imagers B and C have detector gains that are adjusted automatically in response to changes in the scene being imaged. The measured values of the transmission with one and two sprays in the optical path are $\tau = 0.839$ with $s = 0.020$ and $\tau = 0.710$ with $s = 0.015$, respectively. Note that imager A is sensitive to radiation over the wavelength range from 3.4 to 5.0 μm. Thus, the data represents an average transmission over this range.

The predictions presented in Fig. 7 indicate that the transmission does not vary significantly with wavelength. This is consistent with the previously reported data obtained with the infrared spectrograph [6]. As shown in Fig. 7, the transmission measurements obtained with imager A are consistent with the theoretical predictions (including in-scattering) and previous measurements. This suggests that imager A can measure the transmission through water sprays with reasonable accuracy.

Laser extinction measurements were also obtained through the water sprays for comparison with the data obtained at infrared wavelengths. The transmission at $\lambda = 0.6328$ μm was measured to be $\tau = 0.805$ with $s/\sqrt{N} = 0.0001$ and $\tau = 0.660$ with $s/\sqrt{N} = 0.0023$ for one and two spray, respectively. The transmission data obtained from the laser extinction measurements are also presented in Fig. 7.

The two fire fighter thermal imagers (imagers B and C) do not show a noticeable decrease in the contrast of the target image as sprays are introduced into the optical path. These imagers are designed to automatically adjust the detector gain and iris opening in response to varying levels of radiation intensity falling upon the detector. This feature is intended to permit fire fighters to use the devices without the need for

manual adjustments. One noteworthy feature of the images presented in Fig. 6 is that although the image of the target does not appear to deteriorate due to the water sprays, the contrast between the background and the target decreases. This is a result of the automatic adjustments that are made in response to lower levels of radiation falling on the detector.

4.2. Image quality metrics

It is desirable to quantify the effect of participating media such as smoke and water sprays on the thermal imager performance. There are numerous metrics that can be used to evaluate the quality of infrared imaging systems. Some examples include: (i) the aperiodic transfer function (ATF), (ii) the signal transfer function (SiTF), (iii) the optical transfer function (OTF) composed of the modulation transfer function (MTF) and the phase transfer function (PTF), and (iv) the contrast transfer function (CTF) [1]. Because the objective of this study is to explore the effect of the participating media on the imaging system's performance, some metrics will be more suitable than others. For example, metrics that quantify the spatial resolution of the system will be less appropriate than metrics that quantify the image contrast because participating media will affect the image contrast but not the spatial resolution of the imaging system.

The SiTF is an input-to-output transformation, and is determined by varying the target intensity with fixed target size and monitoring the responsivity of the imaging system. The SiTF is reported to be a poor metric for comparing different systems because it changes with gain. Because most fire fighter thermal imagers have automatic gains, this would be a difficult metric to measure and interpret for such imaging systems.

The ATF is the transformation of input target area to output voltage for fixed target intensity. The ATF does not measure the imaging system's ability to identify detail, but rather it is a metric of the imaging system's ability to measure *something*. This metric is relevant to the ability to detect sources or hot spots, and thus may be a useful metric for evaluating fire fighter thermal imager performance. However, the implementation of the ATF for fire fighter thermal imagers is complicated by the automatic gain and other features designed to simplify the operation of the imagers. The implementation of this metric is currently being explored, but will not be used here.

The OTF is a measure of the imaging system's ability to capture a sinusoidal intensity profile. The MTF is the magnitude and the PTF is the phase of the complex OTF. For an ideal system viewing incoherent radiation, the OTF is real and the OTF and MTF are equal. The MTF is attractive as a metric for the current study because it does not depend upon the system gain. Furthermore, there is a large body of literature relating the MTF to the performance of imaging systems operating at visible wavelengths. To measure the MTF, a target is used in which the intensity varies sinusoidaly in one dimension. A more convenient image quality metric is the CTF, which is the system response to a square-wave target. The alternating hot and cold lines of the target used in this study represent such a square wave target. The

CTF and MTF are calculated using the same formula, with the only difference being the input target. To calculate the CTF from an image of a square-wave target, the following formula is used:

$$\mathrm{CTF} = \frac{I_{\max} - I_{\min}}{I_{\max} + I_{\min}}, \tag{3}$$

where $I_{\min}$ and $I_{\max}$ are defined in Fig. 8. The MTF and CTF are measures of an imaging system's ability to transfer contrast from the object to the image. It should be noted that the measured MTF and CTF apply only to the particular resolution level of the target. Thus, in general, it is useful to determine these metrics at different resolution levels when evaluating the performance of imaging systems. Because the objective of the current study is to explore the effect of the water sprays on the image quality, the CTF will be evaluated with and without sprays in the optical path and compared at a single resolution only.

Fig. 9 presents mean (horizontal) intensity profiles across the targets obtained with the three thermal imagers. The intensity profiles were obtained from the data in Fig. 6 corresponding to no spray in the optical path. The intensity profiles correspond to the gray-scale intensity of the images and are presented in arbitrary units. The horizontal coordinate is given in pixels. Note that the intensity profile of imager A appears to have sub-pixel level variations. This is because the imager is equipped with an electronic zoom feature. This feature increases the magnification of the display, but does not change the field of view. Thus, the spatial resolution of the imager is not increased. Imager A does, however, have a smaller field of view than imagers B and C (see Table 1). Thus the spatial resolution of this imager is greater than that of the other imagers.

The data in Fig. 9 indicate significant variation in the intensity profiles between the three imagers. This is further illustrated in Fig. 10, where the calculated CTF is presented. Note that the error bars in Fig. 10 correspond to the standard deviation of replicated measurements. The quantitative metric presented in Fig. 10 correlates strongly with the qualitative appearance of the images in Fig. 6 and the intensity profiles in Fig. 9. As noted above, the CTF does not depend upon the system gain

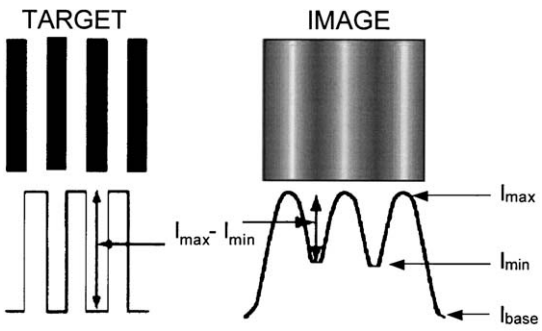

Fig. 8. Parameters used to calculate the modulation transfer function (MTF) and the contrast transfer function (CTF).

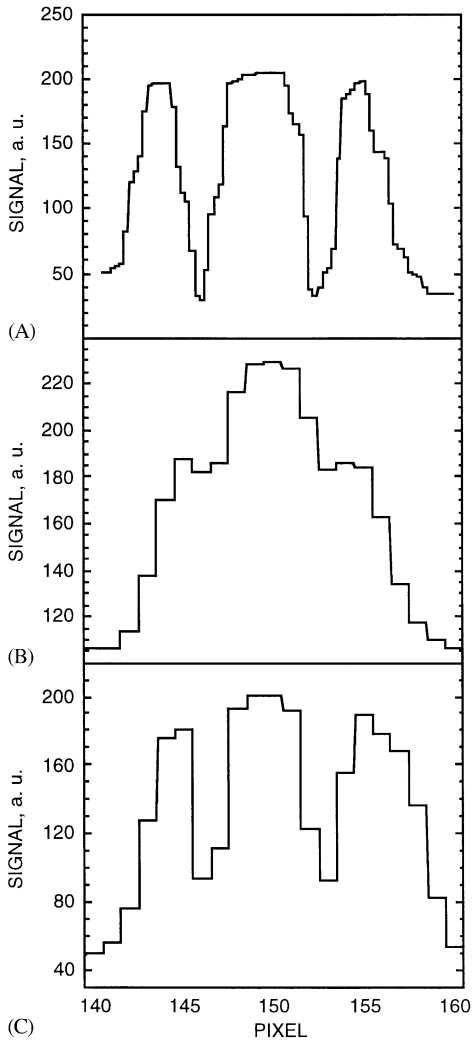

Fig. 9. Mean intensity profiles for (A) imager A, (B) imager B, and (C) imager C obtained from Fig. 5 without a spray in the optical path.

and is therefore a useful metric for quantifying the effect of participating media on thermal imager performance. The data in Fig. 10 indicate that the image contrast decreases as the sprays are introduced into the optical path for imager A, but the sprays do not have an effect on the image quality for imagers A and B. This is consistent with the qualitative evaluation of the images in Fig. 6. The values of the CTF presented in Fig. 10 also "rank" correctly the quality of the images obtained from the three thermal imagers that are presented in Fig. 6.

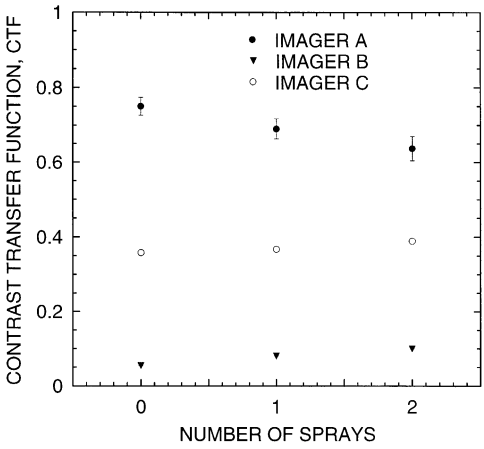

Fig. 10. Calculated contrast transfer function (CTF) corresponding to the data presented in Fig. 6.

4.3. Full-scale tests

In addition to the laboratory-scale tests reported above, the effect of water sprays produced by fire sprinklers on thermal imager performance was investigated. To relate the full-scale tests to the more controlled laboratory-scale tests, it is useful to consider the predicted transmission through such water sprays. Unfortunately, experimental determination of drop size distributions and number densities throughout a full-scale spray is a difficult, costly, and time-consuming task, and such information is not available for the sprinklers used here. However, Widmann [9] measured the characteristics of water sprays produced by four residential sprinklers using PDI, and calculating the predicted transmission of radiation through those sprays can provide insight into the relation between the laboratory- and full-scale tests conducted here. Using Eq. (2), the size distributions and drop number density data from that study, and the optical extinction efficiencies presented in Fig. 4, the transmission through the sprays can be predicted. Fig. 11 presents the predicted transmission (neglecting forward- and in-scattering) with respect to wavelength for each of the four sprinklers characterized in that study. The sprinkler characteristics are summarized in Table 2. Note that the predicted transmission varies from approximately $\tau = 0.2$ to less than $\tau = 0.01$. Thus, the extinction of infrared radiation by water sprays produced by fire sprinklers is significantly greater than the extinction due to the laboratory-scale spray discussed above. It should be emphasized that the transmission data in Fig. 11 applies to imaging applications, but for radiative heat transfer calculations the effects of in- and forward-scattering should be included.

The flow rate determined from the K-factor [15] and operating pressure for each sprinkler is presented in Table 2. It is interesting to note that the extinction predictions presented in Fig. 11 do not correlate with the total flow rate through the nozzle. The greatest extinction is predicted for the water spray produced by

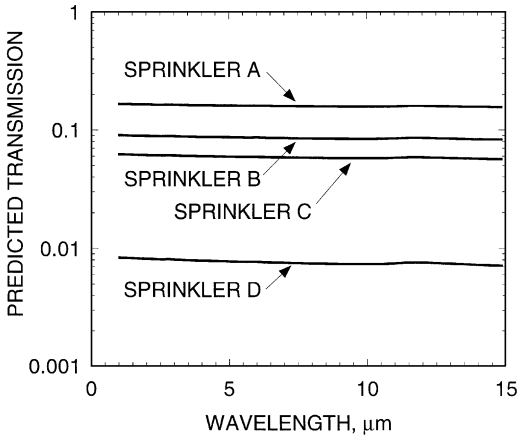

Fig. 11. Predicted transmission, I/I_0, through the water sprays produced by four residential sprinklers. Drop size and number density data are from Ref. [9].

Table 2
Sprinklers used in this study

Sprinkler	Type	*K*-factor	Pressure	Calculated flow rate
A	Pendent	$0.72\times10^{-4}\,m^3\,s^{-1}\,kPa^{-0.5}$ ($3.0\,gal\,min^{-1}\,psi^{-1}$)	$103\pm7\,kPa$ ($15\pm1\,psi$)	$0.73\times10^{3}\pm0.05\times10^{3}\,m^3\,s^{-1}$ ($11.6\pm0.8\,gal\,min^{-1}$)
B	Pendent	$1.35\times10^{-4}\,m^3\,s^{-1}\,kPa^{-0.5}$ $5.6\,gal\,min^{-1}\,psi^{-1}$)	$131\pm7\,kPa$ ($19\pm1\,psi$)	$1.54\times10^{3}\pm0.05\times10^{3}\,m^3\,s^{-1}$ ($24.4\pm0.8\,gal\,min^{-1}$)
C	Pendent	$1.35\times10^{-4}\,m^3\,s^{-1}\,kPa^{-0.5}$ ($5.6\,gal\,min^{-1}\,psi^{-1}$)	$131\pm7\,kPa$ ($19\pm1\,psi$)	$1.54\times10^{3}\pm0.05\times10^{3}\,m^3\,s^{-1}$ ($24.4\pm0.8\,gal\,min^{-1}$)
D	Pendent	$0.75\times10^{-4}\,m^3\,s^{-1}\,kPa^{-0.5}$ ($3.1\,gal\,min^{-1}\,psi^{-1}$)	$172\pm7\,kPa$ ($25\pm1\,psi$)	$0.98\times10^{3}\pm0.05\times10^{3}\,m^3\,s^{-1}$ ($15.5\pm0.8\,gal\,min^{-1}$)
E	Pendent	$1.03\times10^{-4}\,m^3\,s^{-1}\,kPa^{-0.5}$ ($4.3\,gal\,min^{-1}\,psi^{-1}$)	$103\pm7\,kPa$ ($15\pm1\,psi$)	$1.05\times10^{3}\pm0.05\times10^{3}\,m^3\,s^{-1}$ ($16.7\pm0.8\,gal\,min^{-1}$)
F	Upright	$2.68\times10^{-4}\,m^3\,s^{-1}\,kPa^{-0.5}$ ($11.2\,gal\,min^{-1}\,psi^{-1}$)	$103\pm7\,kPa$ ($15\pm1\,psi$)	$2.73\times10^{3}\pm0.08\times10^{3}\,m^3\,s^{-1}$ ($43.4\pm1.4\,gal\,min^{-1}$)
G	Pendent	$6.0\times10^{-4}\,m^3\,s^{-1}\,kPa^{-0.5}$ ($25\,gal\,min^{-1}\,psi^{-1}$)	$103\pm7\,kPa$ ($15\pm1\,psi$)	$6.1\times10^{3}\pm0.05\times10^{3}\,m^3\,s^{-1}$ ($97\pm3.2\,gal\,min^{-1}$)

sprinkler D even though the total flow rate of water is greater for sprinklers B and C. This is because the water sprays produced by sprinkler D display drop size distributions weighted heavily towards the smaller drops. Thus, the number density is higher even though the total flow rate is lower.

Fig. 12 presents images obtained using imager C and sprinklers E, F, and G. Note that there is a person and a radiant heater on the far side of the spray. The radiant

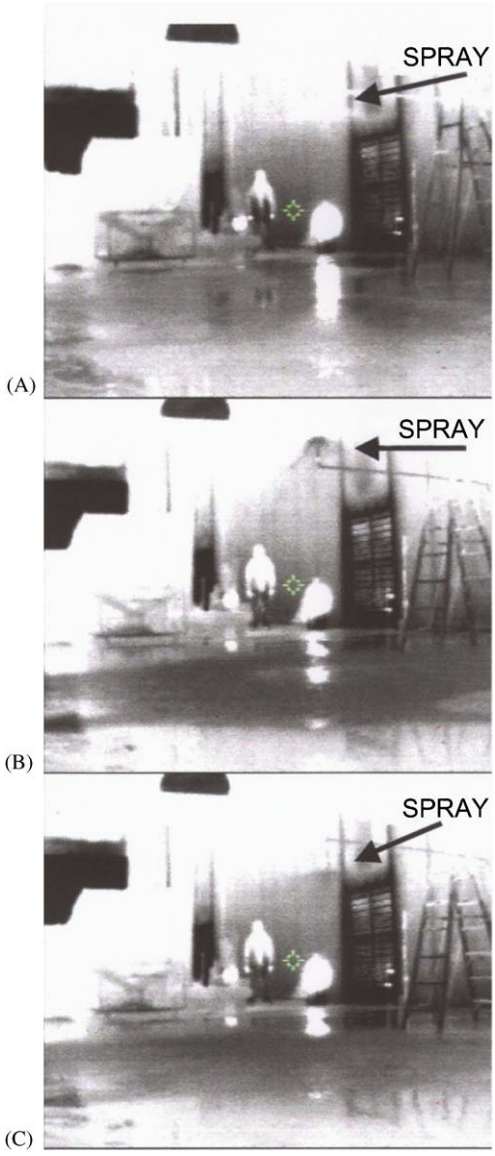

Fig. 12. Images obtained with imager C through water sprays produced by (A) sprinkler E, (B) sprinkler F, and (C) sprinkler G.

heater is present to mimic a fire source. Also, the sprays are noticeable in the images and arrows are used to identify them. In all three cases, the imagers are able to successfully penetrate the water spray. The total flow rate of water increases when going from Fig. 12A–C, which is summarized in Table 2. Note that the flow rate through sprinkler E is approximately equal to that of sprinkler D, while the flow rate

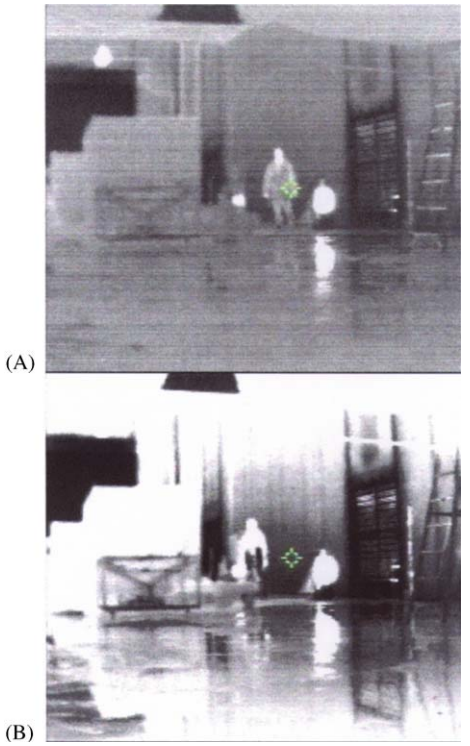

Fig. 13. Images obtained with imager C in the absence of a water spray showing the effect of (A) a dry floor and (B) a wet floor.

through sprinkler G is approximately six times higher. Despite the very high flow rate of water through sprinkler G, the image contrast is sufficient to identify the person and radiant heater on the far side of the spray.

Fig. 13 presents images obtained in the absence of a water spray. Fig. 13A corresponds to an image taken with a dry floor, whereas Fig. 13B corresponds to an image collected with water on the floor. The thermal imager automatically compensates for the increased dynamic range required to image both the floor and the targets (person and radiant heater). The images demonstrate the effect of the variable gain. In this case, the image quality of the person is significantly reduced. The variable gain and electronic iris are important features of fire fighter thermal imagers. However, the images presented in Fig. 13 demonstrate that they can have a significant effect upon the image quality, which is an area in need of additional study.

5. Conclusion

The effect of water sprays on fire fighter thermal imagers was explored by intentionally introducing sprays into the optical path. Laboratory-scale tests were

performed using a well-defined target such that the contrast transfer function (CTF) could be calculated. The CTF was found to decrease with decreasing transmission (increasing number water sprays in the optical path) for a scientific infrared imager; however, the CTF for fire fighter thermal imagers was found to be relatively independent of the number of sprays in the optical path over the range of transmissions studied. This was attributed to the automatic gain and electronic iris features incorporated into these imagers.

Full-scale tests were performed with water sprays produced by fire sprinkler nozzles. The *K*-factors for these nozzles ranged from $1.03 \times 10^{-4}\,m^3\,s^{-1}\,kPa^{-0.5}$ ($4.3\,gal\,min^{-1}\,psi^{-1}$) to $6.0 \times 10^{-4}\,m^3\,s^{-1}\,kPa^{-0.5}$ ($25\,gal\,min^{-1}\,psi^{-1}$). The image quality was not found to deteriorate significantly with any of the water sprays. The effect of a water spray in a burning enclosure, where the spray could result in mixing of the hot and cool smoke layers, was not investigated but is a topic for future study.

Acknowledgements

The authors would like to thank Laurean Delauter and Jay McElroy for their assistance with the fabrication of the experimental facility.

Appendix A

Extinction efficiencies are given in Table 3.

Table 3
Calculated extinction efficiencies, Q_{ext}, for water drops

Drop diameter, μm							
λ, μm	10	50	100	500	1000	2000	3000
1.02	2.00	2.12	2.06	2.01	2.01	2.01	2.01
1.06	2.22	2.04	2.02	2.02	2.01	2.00	2.00
1.11	2.55	2.04	2.07	2.01	2.01	2.01	2.00
1.15	2.52	2.13	2.07	2.02	2.01	2.01	2.00
1.29	2.27	2.02	2.04	2.01	2.01	2.01	2.00
1.43	1.97	2.11	2.08	2.02	2.01	2.01	2.01
1.66	2.54	2.02	2.06	2.02	2.01	2.01	2.01
1.85	2.77	2.02	2.02	2.02	2.01	2.01	2.01
1.94	2.54	2.18	2.05	2.02	2.01	2.01	2.01
2.17	1.94	2.20	2.02	2.02	2.01	2.01	2.01
2.26	1.74	2.02	2.05	2.03	2.02	2.01	2.01
2.50	2.20	2.04	2.03	2.03	2.02	2.01	2.01
2.59	2.83	2.15	2.08	2.03	2.02	2.01	2.01
2.77	2.25	2.11	2.07	2.03	2.02	2.01	2.01
2.91	2.25	2.11	2.07	2.03	2.02	2.01	2.01
3.00	2.33	2.13	2.08	2.03	2.02	2.01	2.01

Table 3 (*continued*)

Drop diameter, μm							
λ, μm	10	50	100	500	1000	2000	3000
3.14	2.40	2.14	2.09	2.03	2.02	2.01	2.01
3.47	1.95	2.20	2.09	2.03	2.02	2.01	2.01
3.74	2.70	2.29	2.07	2.03	2.02	2.01	2.01
3.97	3.23	2.04	2.09	2.04	2.02	2.01	2.01
4.71	3.69	2.11	2.13	2.04	2.03	2.02	2.01
5.18	3.60	2.31	2.17	2.04	2.03	2.02	2.01
5.45	3.35	2.30	2.10	2.05	2.03	2.02	2.01
5.73	2.75	2.13	2.13	2.05	2.03	2.02	2.01
5.92	2.31	2.22	2.13	2.05	2.03	2.02	2.01
6.06	2.49	2.20	2.13	2.05	2.03	2.02	2.01
6.19	2.98	2.22	2.14	2.05	2.03	2.02	2.01
6.43	3.11	2.24	2.15	2.05	2.03	2.02	2.02
6.89	2.75	2.18	2.15	2.05	2.03	2.02	2.02
7.35	2.42	2.31	2.17	2.05	2.03	2.02	2.02
7.81	2.12	2.39	2.17	2.06	2.04	2.02	2.02
8.74	1.58	2.22	2.20	2.06	2.04	2.02	2.02
9.66	1.14	2.25	2.18	2.06	2.04	2.03	2.02
10.60	0.85	2.44	2.18	2.06	2.04	2.03	2.02
11.50	0.98	2.09	2.11	2.05	2.04	2.02	2.02
12.00	1.15	2.07	2.10	2.05	2.04	2.03	2.02
12.40	1.34	2.11	2.12	2.06	2.04	2.03	2.02
13.70	1.66	2.21	2.16	2.07	2.05	2.03	2.02
14.80	1.81	2.26	2.19	2.08	2.05	2.03	2.03

References

[1] Holst GC. Testing and evaluation of infrared imaging systems. Winter Park, FL, USA: JCD Publishing; 1998.
[2] Bransden BH, Joachain CJ. Introduction to quantum mechanics. New York, NY, USA: Wiley; 1992.
[3] van de Hulst HC. Light scattering by small particles. Toronto, Canada: General Publishing Company; 1957.
[4] Widmann JF. Evaluation of the Planck mean absorption coefficients for radiation transport through smoke. Combust Sci Technol 2003;175:2299–308.
[5] Mie G. Optics of turbid media. Ann Phys 1908;25:377–445.
[6] Widmann JF. Measurement and prediction of infrared radiation attenuation by water sprays. Int J Heat Mass Transfer, submitted for publication.
[7] Bayvel LP, Jones AR. Electromagnetic scattering and its applications. Englewood, NJ: Applied Science Publishers Ltd.; 1981.
[8] Widmann JF. Characterization of a residential fire sprinkler using phase Doppler interferometry. Atomizat Sprays 2002;11:69–90.
[9] Widmann JF. Phase Doppler interferometry measurements in water sprays produced by residential fire sprinklers. Fire Saf J 2001;36:545–67.
[10] Dembele S, Wen JX, Sacadura JF. Analysis of the two-flux model for predicting water spray transmittance in fire protection application. Trans ASME J Heat Transfer 2000;122:183–6.
[11] Kerker M. The scattering of light and other electromagnetic radiation. London: Academic Press; 1961.

[12] Bohren CF, Huffman DR. Absorption and scattering of light by small particles. New York: Wiley; 1983.
[13] Segelstein D. The complex refractive index of water. MS thesis, University of Missouri, Kansas City, KS, 1981.
[14] Holst GC. Common sense approach to thermal imaging. Winter Park, FL, USA: JCD Publishing; 2000.
[15] Fleming RP. Automatic sprinkler system calculations. In: The SFPE handbook of fire protection engineering, 2nd ed. National Fire Protection Association, Quincy, MA, June 1995.